J. Fluid Mech. (1984), *vol.* 149, *pp.* 477–501
Printed in Great Britain

Studies on boundary-layer separation in unsteady flows using an integral method

By MICHINORI MATSUSHITA, SHIGERU MURATA AND TERUAKI AKAMATSU

Department of Mechanical Engineering, Kyoto University, Japan

(Received 5 March 1984)

A new two-parameter integral method is presented which is applicable to unsteady two-dimensional laminar boundary layers whether they are separated or not. The governing equations consist of three moments of the boundary-layer equation, and the assumed velocity profiles are those of unsteady trailing-edge flow and Falkner–Skan flow with slip. The governing equation system being hyperbolic, the spontaneous generation of a singularity associated with unsteady separation is confirmed as the focusing of characteristics. The obtained results of the boundary-layer quantities as well as the generation of separation singularity are in good agreement with those of exact methods (e.g. van Dommelen & Shen 1980) for starting flows of cylinders.

1. Introduction

For steady two-dimensional boundary-layer flow, separation is defined by the point of vanishing wall shear, and reversed flow exists adjacent to the wall downstream of this point. It also happens to be a singular point of the solutions of the boundary-layer equation with prescribed pressure distribution, and numerical solutions blow up as this point is approached. The singularity is an exaggerated simulation of the actual rapid thickening of the boundary layer, and the occurrence of the singularity indicates the need for local modifications in the boundary-layer problem. Interactive boundary-layer theory, taking account of the modification of pressure distribution by the presence of boundary layers themselves, gives solutions of separated and reattached flows free of singularity (Williams 1977).

In unsteady boundary-layer flow with a prescribed pressure distribution, the point of vanishing wall shear or onset of reversed flow has no special significance, unlike steady flow, nor is it a singular point in general. This fact has been established through a number of analyses and calculations, as reviewed by Sears & Telionis (1975), Williams (1977) and Telionis (1981). We should also refer to the works of Proudman & Johnson (1962) and Nagata, Minami & Murata (1979). Proudman & Johnson analysed the boundary-layer growth near a rear stagnation point on a cylinder set into motion impulsively from rest and observed that the initial-value problem has a well-behaved solution for all finite time, regardless of the vanishing wall shear and the subsequent reversed flow predicted by the classical series solution. Nagata *et al.* made a visualization study of starting flow of a circular cylinder using both hydrogen-bubble techniques and electrolysis methods. They confirmed that the location and time of the first appearance of reversed flow, which is detected by the hydrogen-bubble technique, are in good agreement with the classical theory and that the initial stage of the reversed flow does not lead to an abrupt thickening nor breakaway of the boundary layer. Furthermore, they observed by the electrolysis

method that the ejection of vorticity produced on the body surface toward the external stream occurs farther after the first appearance of reversed flow.

Sears & Telionis (1975) contended that blow-up of the unsteady boundary-layer solution for a prescribed pressure distribution, rather than reversal of flow direction at the wall, signals the termination of boundary-layer type flow and that this phenomenon is the natural generalization of 'boundary-layer separation' to the unsteady flow. They also advocated that it appears at the so-called MRS point where both streamwise velocity u and shear $\partial u/\partial y$ simultaneously vanish in a coordinate system moving with separation. In order to verify the MRS and singularity hypothesis, Telionis & Tsahalis (1974) performed a numerical integration of the boundary-layer equations in a number of flows, one of which is starting flow of a circular cylinder. For this problem they reached the conclusion that a singularity appears at $t = 0.65$ and $\theta = 140°$. On the other hand, Cebeci (1979), after repeating this calculation by a Box scheme combined with a zigzag procedure, rightly claimed that the boundary layer is smooth at $t = 0.65$ and that their 'singularity' is a consequence of the numerical method. Nevertheless, after some controversy, the singularity hypothesis has ultimately been established by van Dommelen & Shen (1980). The history of the controversy is reviewed by Telionis (1981), Cebeci (1982), van Dommelen & Shen (1982) and Wang (1982). Employing Lagrangian coordinates instead of the usual Eulerian ones, van Dommelen & Shen (1980, 1982) verified that the singularity appears at $t = 1.50$ and $\theta = 111°$ and derived an analytic structure of the singularity in the starting flow of a circular cylinder. Cowley (1983) confirmed the results of van Dommelen & Shen by recasting the classical series solution using rational functions. Wang (1982) contended that, just as in three-dimensional separation, the envelope of analogous limiting streamlines represents unsteady separation, and found out the location of separation fairly close to that of van Dommelen & Shen. Though the definition of Wang's analogy criterion of unsteady separation has no connection with singularity, it coincides with symptoms of singularity, such as rapid growth of boundary-layer thickness or sharp increase of normal velocity.

Without analytical solution, it may not be straightforward to know where the singularity is located by the conventional numerical method. Van Dommelen & Shen elucidated that a stationary point in the Lagrangian dependent variable x implies a singular point in the dependent variable y through the continuity equation, and then u_x blows up at this point. Cowley obtained an approximate analytic continuation of the extended classical series solution using continuous fractions and confirmed the development of the singularity by the presence of a simple pole on the positive real axis in the complex-time plane. In this way they successfully represented the singularity by a stationary point in the Lagrangian variable or a simple pole of a rational function, which can be captured by numerical calculations without blow-up. Previous to these convincing pieces of evidence, Shen (1978), employing the patching procedure, drew the qualitative conclusion that wall shear can develop a singularity analogous to shock formation through a coalescence of characteristics. However, he could not give a quantitative answer, and mentioned the necessity of a momentum-integral formulation for reasonable accuracy and general applicability.

One of the earliest and, until recently, most widely used approximate methods for the solution of boundary-layer equations is the momentum-integral method using one-parameter velocity profiles developed by Pohlhausen (1921). Schuh (1953) applied it to a general class of unsteady boundary layers including starting flow of a circular cylinder by reducing the momentum-integral equation to two simultaneous

ordinary differential equations, one of which is an 'equation of characteristics'. However, this method, giving reasonably accurate solutions in accelerated flow, has defects in that it fails for a strong adverse pressure gradient and predicts separation too late. For better accuracy, Tani (1954) employed an energy-integral equation in addition to the momentum integral and dropped the compatibility condition on the wall. Lees & Reeves (1964) successfully applied Tani's two-moment one-parameter integral method to a separating and reattaching laminar flow of boundary-layer–shock-wave interaction. Tani & Yu (1971) solved unsteady boundary layers by the two-moment method, specifying functional relations among the shape parameters directly without recourse to any specific velocity profiles. Matsushita & Akamatsu (1983) modified Tani's method and applied it to the starting flow of a circular and an elliptic cylinder and obtained good results except for the region of large reversed flow.

In this paper, extending Tani's method, we propose a two-parameter integral method which is applicable to two-dimensional laminar boundary layers whether they are separated or not. The second moment of the boundary-layer equation, obtained by integrating the boundary-layer equation multiplied by u^2 across the layer, is employed as a governing equation in addition to the zeroth- and first-moment equations, i.e. momentum and energy integrals. The assumed velocity profiles are composed of two families: one is Falkner–Skan flow with slip, and the other is semisimilar trailing-edge flow analysed by Williams (1982). The governing equation system being hyperbolic, a singular behaviour of an unsteady boundary layer with prescribed pressure distribution, such as, $\partial\delta_1/\partial x \to \infty$, is reducible to the formation of a shock-like discontinuous solution through the coalescence of characteristics, as conjectured by Shen (1978). Within the framework of the one-parameter integral method, this fact has already been confirmed by Matsushita & Akamatsu (1984). For turbulent boundary layers, Cousteix & Houdeville (1981) found that the similar singularities are formed in the system of the entrainment and momentum integral. In order to capture the discontinuity, we utilize a dissipative finite-difference scheme, which is a familiar method in gas-dynamics, and examine the behaviour of characteristics. Thus we can numerically confirm the appearance of singularity without troublesome blow-up, as van Dommelen & Shen and Cowley have succeeded in doing by their own methods. Further, the present method gives an efficient and practical prediction of separation without stepwise computation of the complete boundary-layer equation.

2. Governing equations

The basic equations for unsteady two-dimensional incompressible boundary layers are:

$$\frac{\partial u}{\partial t}+u\frac{\partial u}{\partial x}+v\frac{\partial u}{\partial y}=\frac{\partial U}{\partial t}+U\frac{\partial U}{\partial x}+\nu\frac{\partial^2 u}{\partial y^2}, \tag{1}$$

$$\frac{\partial u}{\partial x}+\frac{\partial v}{\partial y}=0, \tag{2}$$

where x and y are distances measured, respectively, along and normal to the surface of the body, t is time, u and v are the velocity components in the x- and y-directions respectively, U is the free-stream velocity just outside the boundary layer and ν is

the kinematic viscosity. The boundary condition on u and v for impermeable walls are:

$$\left.\begin{aligned} u = 0, \quad v = 0, \quad (y = 0), \\ u \to U \quad (y \to \infty). \end{aligned}\right\} \tag{3}$$

The free-stream velocity $U = U(x, t)$ is presumably known from a potential-flow analysis.

Integrating the following equation for $n = 0, 1, 2$ across the boundary layer, we can derive the nth moment of the boundary-layer equation:

$$\text{equation (1)} \times (n+1)\, u^n - \text{equation (2)} \times (U^{n+1} - u^{n+1}).$$

The results are obtained as

$$\frac{\partial}{\partial t}(U\delta_1) + \frac{\partial}{\partial x}(U^2\delta_2) + U\frac{\partial U}{\partial x}\delta_1 = \frac{\tau_w}{\rho}, \tag{4}$$

$$\frac{\partial}{\partial t}(U^2\delta_2) + \frac{\partial}{\partial x}(U^3\delta_3) + U^2\frac{\partial \delta_1}{\partial t} = 2\nu \int_0^\infty \left(\frac{\partial u}{\partial y}\right)^2 \mathrm{d}y, \tag{5}$$

$$\frac{\partial}{\partial t}(U^3\delta_3) + \frac{\partial}{\partial x}(U^4\delta_4) + U^3\frac{\partial \delta_1}{\partial t} - 3U^2\frac{\partial U}{\partial t}\delta_2 - 3U^3\frac{\partial U}{\partial x}\delta_2 = 6\nu \int_0^\infty u\left(\frac{\partial u}{\partial y}\right)^2 \mathrm{d}y. \tag{6}$$

The zeroth and first moments of the momentum equation are termed the momentum and mechanical-energy integrals respectively. Here δ_i $(i = 1, \ldots, 4)$ are boundary-layer thickness defined as follows:

$$\delta_1 = \int_0^\infty \left(1 - \frac{u}{U}\right) \mathrm{d}y, \quad \delta_2 = \int_0^\infty \frac{u}{U}\left(1 - \frac{u}{U}\right) \mathrm{d}y, \tag{7a,b}$$

$$\delta_3 = \int_0^\infty \frac{u}{U}\left(1 - \frac{u^2}{U^2}\right) \mathrm{d}y, \quad \delta_4 = \int_0^\infty \frac{u}{U}\left(1 - \frac{u^3}{U^3}\right) \mathrm{d}y. \tag{7c,d}$$

δ_1, δ_2 and δ_3 are the displacement, momentum and energy thicknesses respectively. The wall shear stress τ_w is defined as

$$\tau_\omega = \mu\left(\frac{\partial u}{\partial y}\right)_{y=0} \tag{8}$$

The following six shape parameters are constructed from the variables appearing in (4)–(6):

$$\left.\begin{aligned} E = \frac{\delta_2}{\delta_1}, \quad F = \frac{\delta_3}{\delta_1}, \quad G = \frac{\delta_4}{\delta_1}, \\ B = \frac{2\delta_1 \tau_w}{\mu U}, \quad S = \frac{2\delta_1}{U^2}\int_0^\infty \left(\frac{\partial u}{\partial y}\right)^2 \mathrm{d}y, \\ Q = \frac{2\delta_1}{U^3}\int_0^\infty u\left(\frac{\partial u}{\partial y}\right)^2 \mathrm{d}y. \end{aligned}\right\} \tag{9}$$

The governing equations are rewritten in a non-dimensional conservation form using the above shape parameters:

$$w_t + f_x = z, \tag{10}$$

where
$$\boldsymbol{w} = \begin{bmatrix} \delta_1 \\ (E+1)\,\delta_1 \\ (F+1)\,\delta_1 \end{bmatrix}, \qquad \boldsymbol{f} = \begin{bmatrix} UE\delta_1 \\ UF\delta_1 \\ UG\delta_1 \end{bmatrix}, \tag{11), (12}$$

$$\boldsymbol{z} = \begin{bmatrix} \dfrac{B}{2\delta_1} - \dfrac{\delta_1 U_t}{U} - (E+1)\,\delta_1 U_x \\ \dfrac{S}{\delta_1} - \dfrac{2E\delta_1 U_t}{U} - 2F\delta_1 U_x \\ \dfrac{3Q}{\delta_1} + \dfrac{3(E-F)\,\delta_1 U_t}{U} + 3(E-G)\,\delta_1 U_x \end{bmatrix}. \tag{13}$$

The shape parameters E and F appearing in the unsteady term $\boldsymbol{w}_t$ of the (10) are selected as the independent parameters from among the ones in the (9). The others, G, S, B and Q, are specified as functions of the two parameters E and F through the assumed velocity profile. Then (10), having three unknowns δ_1, E and F, forms a closed governing equation system for the present integral method.

3. Velocity-profile assumption

The assumed velocity profiles in the present integral method are those of Falkner–Skan flows with slip and semisimilar flows in the vicinity of the trailing edge on bodies impulsively set into motion. These flows may be regarded as Falkner–Skan flows extended to unsteady flows or slipping flows so as to make two-parameter velocity-profile families.

3.1. *Falkner–Skan flows with slip*

The governing equation and boundary conditions for the Falkner–Skan flows with slip are as follows:

$$f''' + ff'' + \beta(1 - f'^2) = 0, \tag{14}$$

$$f(0) = 0, \quad f'(0) = U_w, \quad f'(\infty) = 1, \tag{15}$$

which forms a velocity-profile family of two-parameters β and U_w. Though a systematic approach is given for this two-point boundary-value problem by Cebeci & Wilson (1972), we employed a simple shooting method with fourth-order Runge–Kutta method and obtained normalized velocity profiles in a coordinate system moving with a velocity U_w by the transformation $(f' - U_w)/(1 - U_w)$ (figure 1). Figure 2 shows the velocity profiles obtained for $U_w = 0.4$ and various values of β and the shape parameters E and F defined in §2. The velocity profiles have a monotonic correspondence along the curve of $f''(0)$ versus β plotted in figure 2 of Cebeci & Wilson (1972) but not to β itself. We obtained about 200 profiles for 9 values of U_w ranging from 0 to 0.8. In figure 5 pairs of E and F calculated from each velocity profile are plotted with triangular symbols. They are employed as input data for the interpolation of dependent parameters in §3.3.

3.2. *Trailing-edge flow*

Williams (1982) has elucidated that boundary-layer flows in the vicinity of the sharp trailing edge of a symmetrical body (figure 3) impulsively set into motion have semisimilar solutions. They are also employed as the assumed velocity profile in the

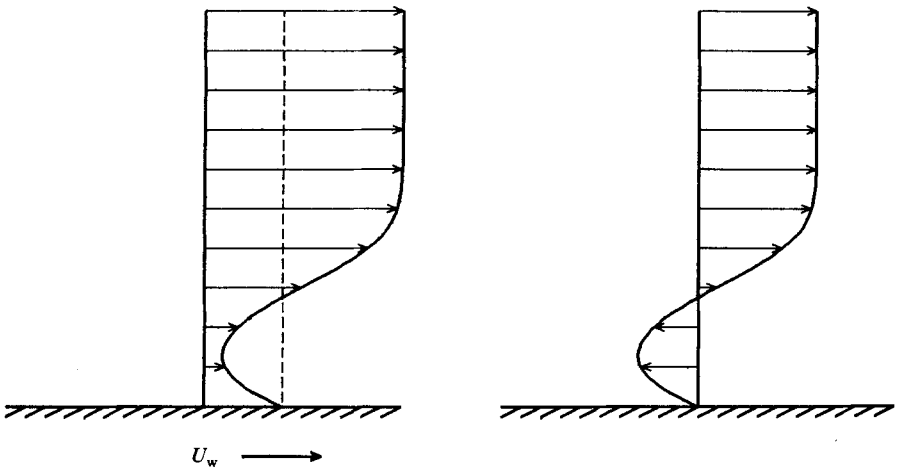

FIGURE 1. Schematic velocity profile with slip velocity U_w (left) and the corresponding profile seen in a coordinate system moving with the velocity U_w.

$U_w = 0.4$

	β	E	F
1	−0.35	−0.203	−0.039
2	−0.42	−0.011	0.105
3	−0.41	0.203	0.320
4	−0.20	0.361	0.564
5	1.00	0.457	0.745

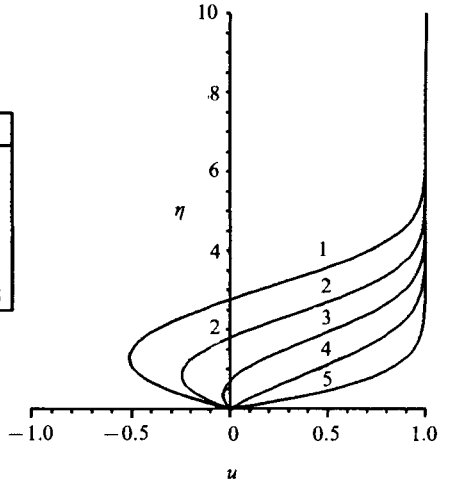

FIGURE 2. Velocity profiles obtained from Falkner–Skan flow with slip for several values of β ($U_w = 0.4$).

present integral method. According to Williams, when the internal angle of the trailing edge is $2\pi m/(m+1)$, the free-stream velocity is $-cx^m$ and the three independent variables (x, y, t) can be reduced to the following two variables:

$$\xi = 1-\exp(-cx^{m-1}t), \quad \eta = y\left(\frac{cx^{m-1}}{\nu\xi}\right)^{\frac{1}{2}}. \tag{16}$$

The reduced momentum equation and boundary condition become

$$\frac{\partial^2 w}{\partial\eta^2}+\alpha_1\frac{\partial w}{\partial\eta}+\alpha_2 w+\alpha_3 = \alpha_4\frac{\partial w}{\partial\xi}, \quad \frac{\partial f}{\partial\eta} = w, \tag{17}$$

$$w(\xi,0) = f(\xi,0) = 0, \quad w(\xi,\infty) = 1, \quad w(0,\eta) = \operatorname{erf}(\eta). \tag{18}$$

Here f is a non-dimensional stream function, and the coefficients $\alpha_1, \ldots, \alpha_4$ are given functions of f, ξ, η and m. These equations define a velocity-profile family of

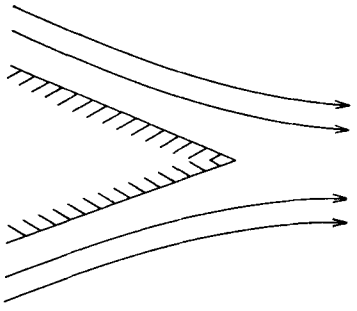

FIGURE 3. Flow geometry for flow near a rear stagnation point.

$m = 0.8$

	ξ	E	F
1	0.991	−0.277	0.106
2	0.965	−0.233	0.083
3	0.891	−0.014	0.146
4	0.666	0.270	0.432
5	0.011	0.413	0.659

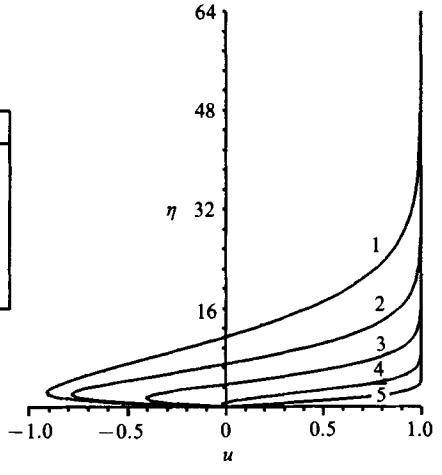

FIGURE 4. Velocity profiles of a rear stagnation flow at several values of ξ ($m = 0.8$).

two-parameters m and the specific variable ξ. We have solved them using an explicit finite-difference scheme proposed by Satofuka & Morinishi (1982) and obtained results for 24 values of m ranging from 0.2 to 1.3. The solutions are terminated at the vanishing of the coefficient α_4. Figure 4 shows the velocity profiles for $m = 0.8$ together with a table of parameters. We obtained about 500 data points from this family, which are plotted in figure 5 with square symbols and also utilized as input data for the interpolation of the dependent parameters.

3.3. *Shape parameters*

As already mentioned, figure 5 shows the plot of the shape parameters E and F obtained from the velocity profiles in §§3.1 and 3.2. Table 1 gives the numerical values of the parameters for five representative data points from among these. Here separation I indicates the Falkner–Skan flow with $U_w = 0$ and $\beta = -0.1988$, and separation II is the trailing-edge flow of $m = 1$ at $\tau = \frac{1}{2}\ln(1-\xi) = 0.32$, both of which have zero wall shear.

Figure 5 indicates that the one-to-one correspondence between E and F existing in the attached-flow region ($E > 0.3$) disappears in the separated-flow region of smaller values of E and F. Figure 6 compares the velocity profiles for a common value of E and different values of F. The velocity profiles for larger values of F have a reversed-flow region nearer the wall and larger peak velocities. Thus it is concluded

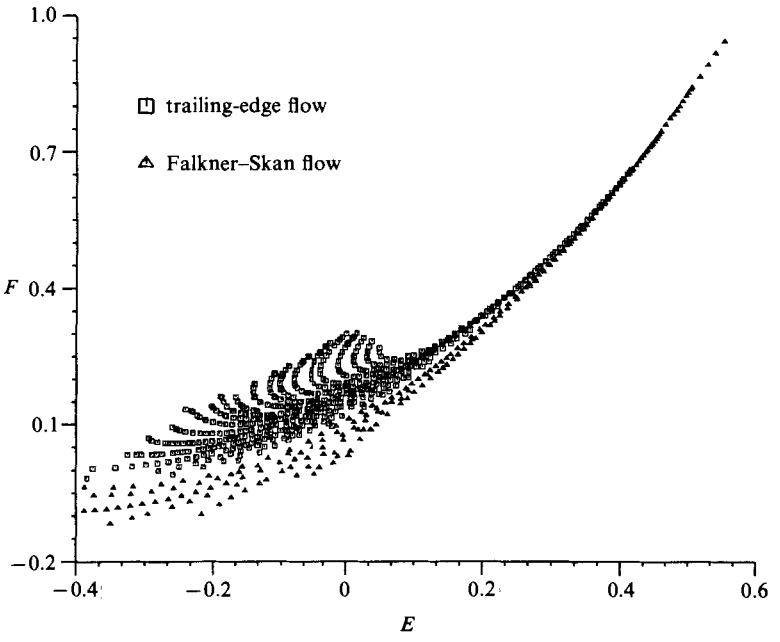

FIGURE 5. Plot of the shape parameters (E, F) obtained from the velocity profiles of Falkner–Skan flow and trailing-edge flow.

	E	F
Hiemenz	0.4512	0.7336
Blasius	0.3859	0.6069
Rayleigh	0.4142	0.6624
Separation I	0.2482	0.3760
Separation II	0.3223	0.5080

TABLE 1. Shape parameters for representative flows

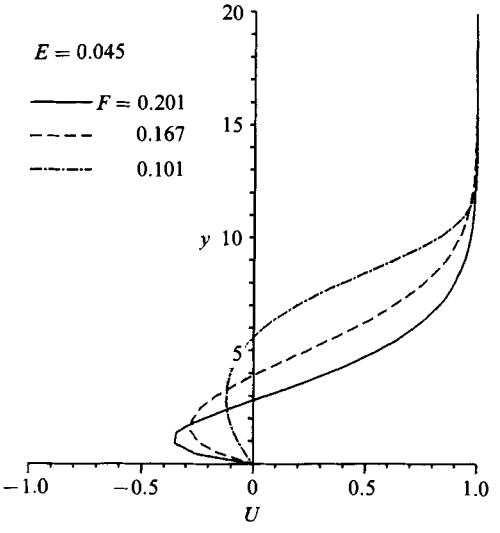

FIGURE 6. Velocity profiles of different values of F for common value of E.

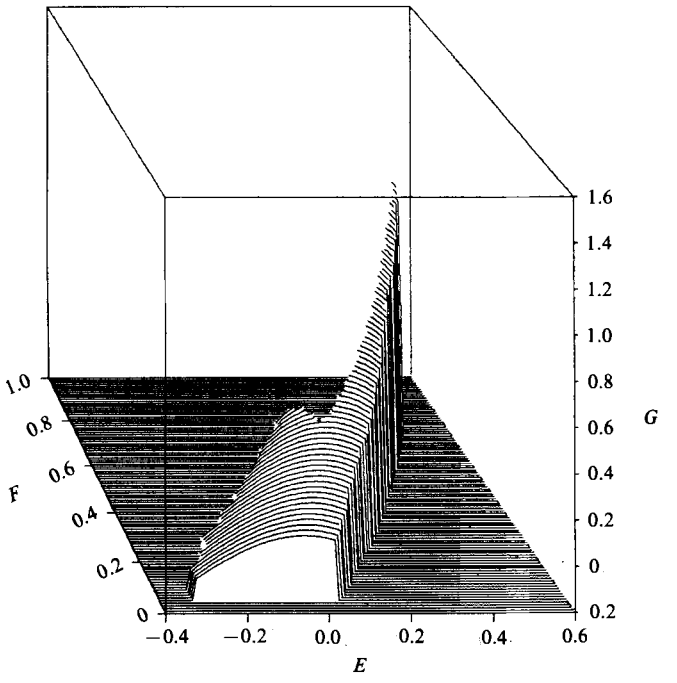

FIGURE 7. Functional relations between independent parameters (E, F) and a dependent parameter G.

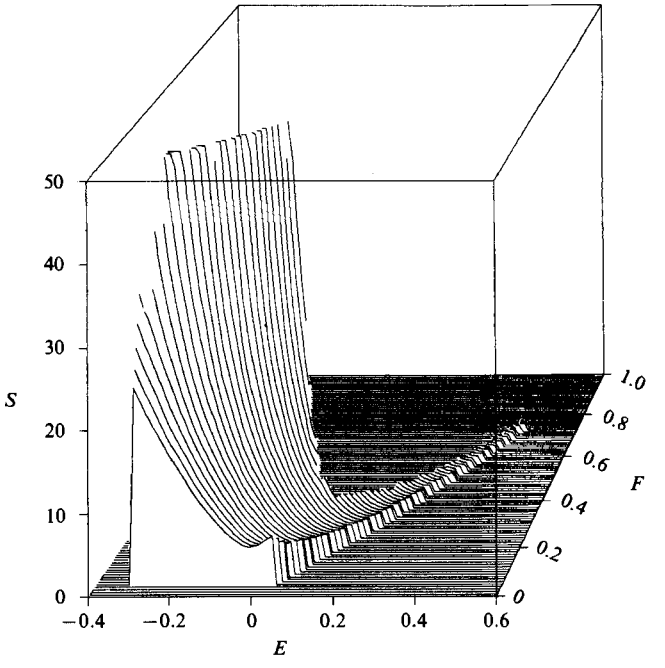

FIGURE 8. Functional relations between independent parameters (E, F) and a dependent parameter S.

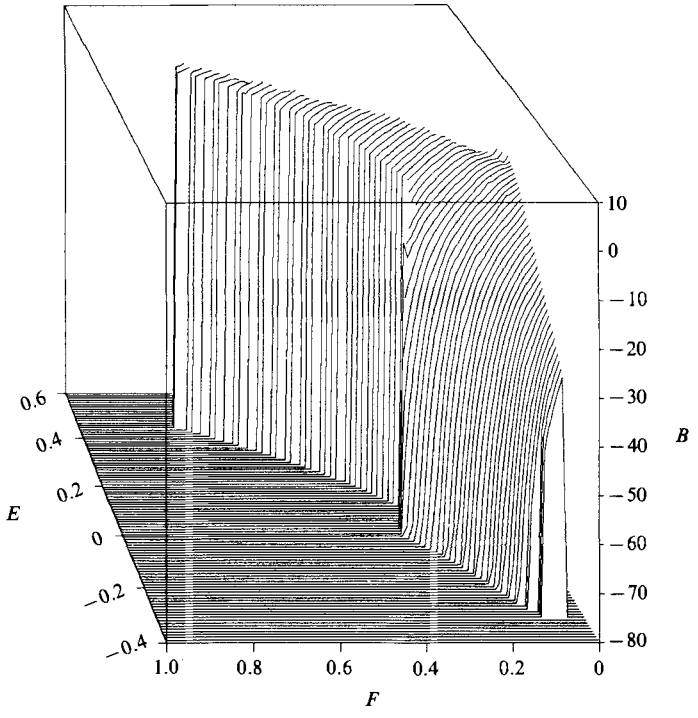

FIGURE 9. Functional relations between independent parameters (E, F) and a dependent parameter B.

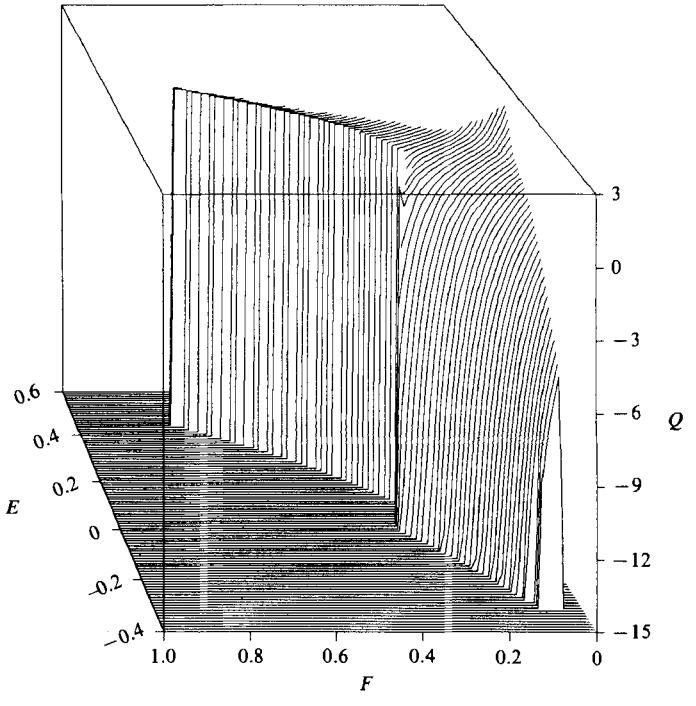

FIGURE 10. Functional relations between independent parameters (E, F) and a dependent parameter Q.

that in separated flows the two-parameter approach is indispensable in the integral method.

The curved surfaces shown in figures 7–10 indicate functional relations between independent parameters E, F and dependent parameters G, S, B, Q (henceforth designated as h). They are obtained by the interpolation of h based on the data points shown in figure 5. The interpolated values of h on the point $(\hat{E}, \hat{F})$ are calculated by locally fitting the following quadratic surface with the data points located at a distance less than some appropriate value r from the point $(\hat{E}, \hat{F})$:

$$h = aE^2 + bEF + cF^2 + dE + eF + f. \tag{19}$$

The coefficients $a, \ldots, f$ are determined by the method of least squares using weighting functions inversely proportional to the distances between data points and the interpolated point $(\hat{E}, \hat{F})$ with a view of obtaining stronger dependence on the nearer data point. The radius r is selected after some trials in order that the circle may include about 20 data points in the attached flow region and about 50 data points in the separated flow region.

4. Nature of governing equations and separation

4.1. *Separation in steady flow*

For steady flow the governing equation (10) becomes $\boldsymbol{f}_x = \boldsymbol{z}$ and may be rewritten as

$$\boldsymbol{A}\frac{\mathrm{d}\boldsymbol{w}}{\mathrm{d}x} = \boldsymbol{z}', \tag{20}$$

where

$$\boldsymbol{A} = U\begin{bmatrix} -1 & 1 & 0 \\ -1 & 0 & 1 \\ G-(E+1)G_E-(F+1)G_F & G_E & G_F \end{bmatrix}, \tag{21}$$

$$\boldsymbol{z}' = \boldsymbol{z} - \begin{bmatrix} E\delta_1 U_x \\ F\delta_1 U_x \\ G\delta_1 U_x \end{bmatrix}. \tag{22}$$

The suffices E and F in (21) denote partial differentiation. The determinant Δ of the coefficient matrix $\boldsymbol{A}$ is

$$\Delta = G - E\frac{\partial G}{\partial E} - F\frac{\partial G}{\partial F}. \tag{23}$$

Figure 11 shows the trajectories of $\Delta = 0$ and $B = 0$ ($\tau_w = 0$) on the (E, F)-plane. The two curves being coincident, the system of governing equations becomes singular at separation in steady flow. As is generally known, this singular behaviour is also observed in the one-parameter integral method (Moses *et al.* 1978; Matsushita & Akamatsu 1983), as well as in the original boundary-layer equation (Goldstein 1948).

As sample calculations, the present method is applied to a linearly retarded flow and a flow past a circular cylinder. The free-stream velocity is $U = 1 - x$ in the former, and the results are shown in figure 12 together with the series solution of Howarth (1938). Figure 13 compares the results of the latter (free-stream velocity $U = 2\sin x$) with the exact numerical solution of Terril (1960). Both of the present results agrees fairly well with the exact solutions, and the separation points of $C_f = 0$ correspond to the singular points of $\Delta = 0$.

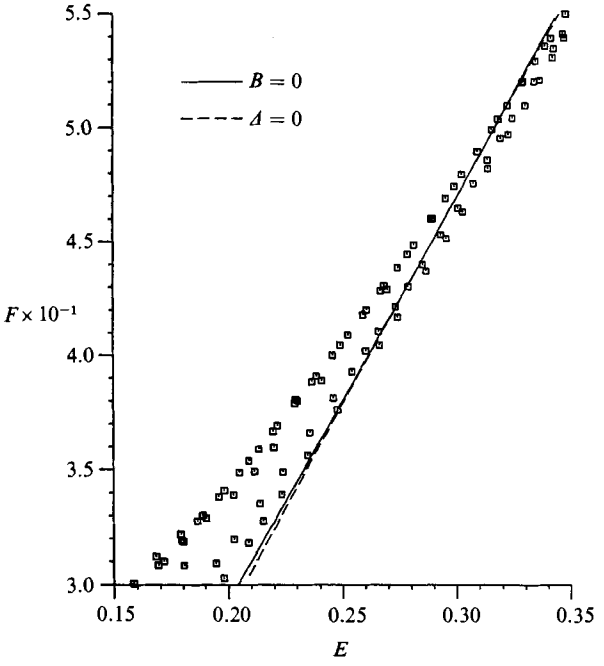

FIGURE 11. Trajectories of $\Delta = 0$ and $B = 0$ on (E, F)-plane.

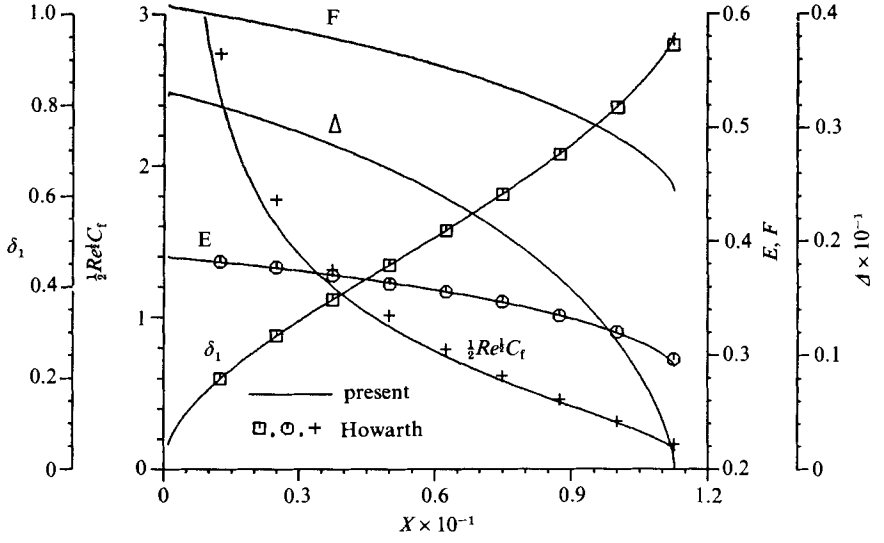

FIGURE 12. Comparison of the present approximate solution with Howarth's exact solution for the case of a linearly retarded flow.

4.2. *Characteristics of governing equations and unsteady separation*

In this subsection some mathematical characteristics of the governing equation system related to unsteady separation are considered. Equations (10)–(13) can be rewritten as a quasi-linear system

$$\boldsymbol{w}_t + \boldsymbol{A}\boldsymbol{w}_x = \boldsymbol{z}', \tag{24}$$

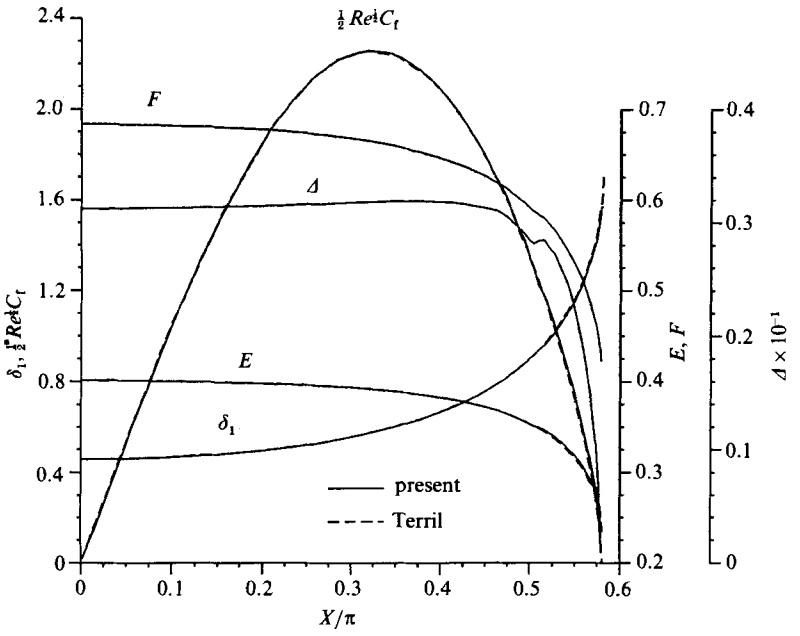

FIGURE 13. Comparison of the present approximate solution with Terril's exact solution for steady flow over a circular cylinder.

where $\boldsymbol{A}$ and z' are given by (21) and (22). The characteristic equation of this system is

$$\det(\boldsymbol{A}-\lambda \boldsymbol{I}) = \lambda^3 + U\left(1-\frac{\partial G}{\partial F}\right)\lambda^2 - U^2\left(1-\frac{\partial G}{\partial E}-\frac{\partial G}{\partial F}\right)\lambda - U^3\left(G-E\frac{\partial G}{\partial E}-F\frac{\partial G}{\partial F}\right) = 0, \tag{25}$$

where $\boldsymbol{I}$ is the unit matrix. Assuming the functional relation between G and (E, F) shown in figure 7, it is confirmed that the characteristic equation always has three distinct real roots and the system is hyperbolic. As mentioned in §4.1, the velocity profiles of zero wall shear ($B = 0$) also have $\Delta = 0$, which corresponds to $\lambda/U = 0$ but not necessarily to a singularity in unsteady flow. Further, the velocity profiles with reversed flow ($B < 0$) have at least one negative characteristic direction, which corresponds to an influence travelling from downstream to upstream. These characteristic families form envelopes on the (x, t)-plane in particular circumstances, across which certain boundary-layer quantities have a discontinuity identified with the separation singularity in unsteady flow. The convective operator in the original boundary-layer equation is responsible for the generation of the singularity, and the diffusion operator merely in the y-direction cannot eliminate it at all. The separation singularity may develop in a finite time in a field initially without singularities, like shock formation in gasdynamics.

5. Results and discussion

The present integral method is applied to the unsteady boundary layers over a circular and an elliptic cylinder impulsively started from rest. In order to solve (10) numerically, the first-order upwind scheme is employed in the attached-flow region,

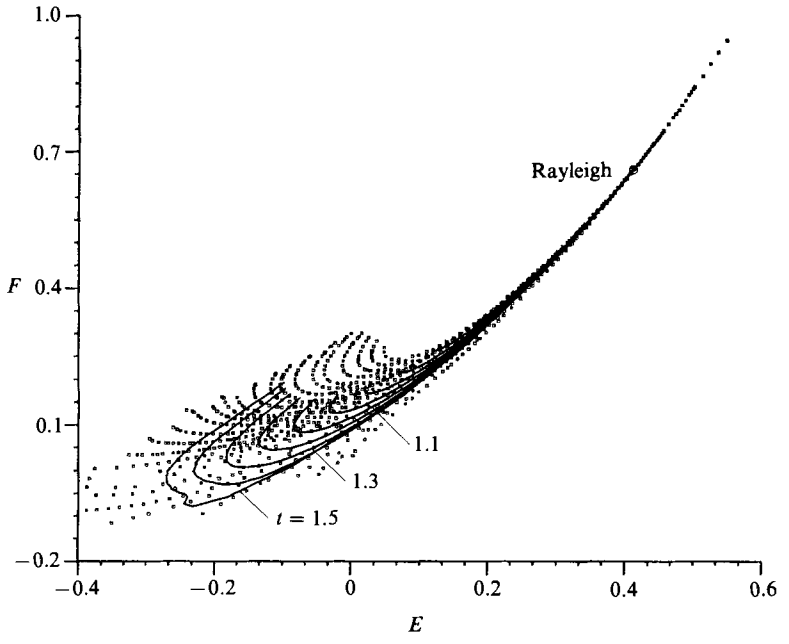

FIGURE 14. The time-varying (E, F)-curve for the starting flow of a circular cylinder impulsively set in motion. The background dots are identical with those in figure 5.

where all the characteristics have positive signs, and the Lax scheme, having central differences in the space direction, is utilized in the reversed-flow region, where the characteristics have mixed signs. For the starting flow of cylinders, there exist full numerical solutions of the Navier–Stokes equations (e.g. Ta Phuoc Loc 1980; Lugt & Haussling 1974) as well as those of the complete boundary-layer equations (Cebeci 1979; van Dommelen & Shen 1980; Telionis & Tsahalis 1974). Both solutions agree for the case of large Reynolds numbers and initial stage of motions. However, at larger times, the boundary-layer solutions assuming an unchangeable free-stream velocity distribution deviate from the Navier–Stokes solutions. The results of the present integral method are compared with the numerical or analytical solutions of the complete boundary-layer equations in the following.

5.1. *Circular cylinder*

The non-dimensional free-stream velocity around the circular cylinder is given by the potential-flow theory as

$$U = 2 \sin x, \tag{26}$$

where x is the streamwise coordinate measured along the surface of the cylinder from the forward stagnation point and normalized by the radius of the cylinder. The free-stream velocity U is normalized by the external flow velocity. Initially the cylinder is assumed to be covered entirely with a boundary layer of Rayleigh type. Then the initial conditions for the present problem are

$$\delta_1 = (B_R \Delta t)^{\frac{1}{2}}, \quad E = E_R, \quad F = F_R, \quad (t = \Delta t), \tag{27}$$

where the suffix R denotes the values for Rayleigh flow shown in table 1. A linear extrapolation is used as a numerical boundary condition. The numerical calculations

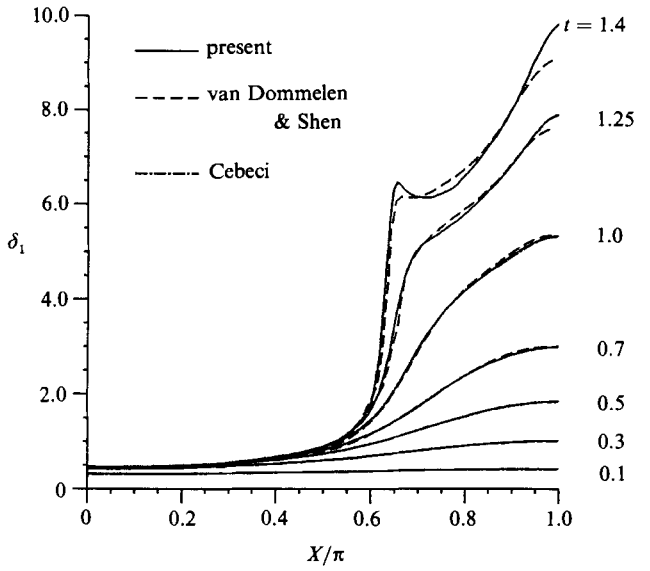

FIGURE 15. The distribution of displacement thickness at various instants for a circular cylinder impulsively set in motion.

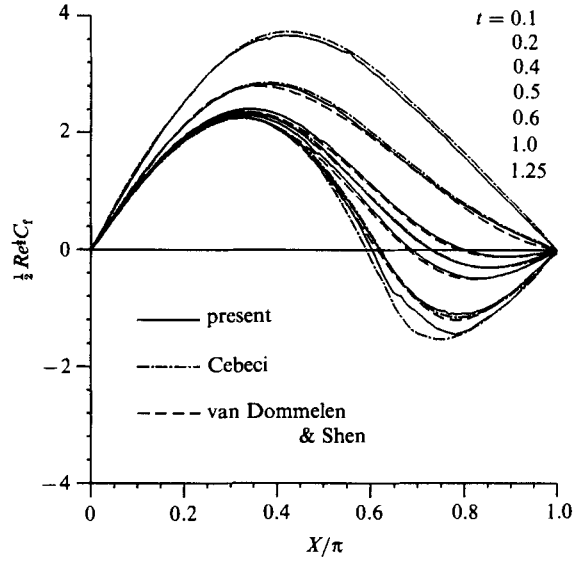

FIGURE 16. The distribution of skin-friction coefficient at various instants for the circular cylinder.

are carried out up to $t = 1.6$ with the step sizes $\Delta t = 0.004$ and $\Delta x = \frac{1}{128}\pi$. The time-varying shape parameters E and F with the interval 0.1 are shown in figure 14 by solid lines. The curve, initially only one point of (E_R, F_R), stretches longer, and gradually the one-to-one correspondence between E and F disappears in largely reversed flow (typically $E < 0$). Thus the one-parameter integral method assuming one-to-one correspondence between E and F turns out to be inappropriate for treating the boundary layer with largely reversed flow. Figure 15 shows the time-varying

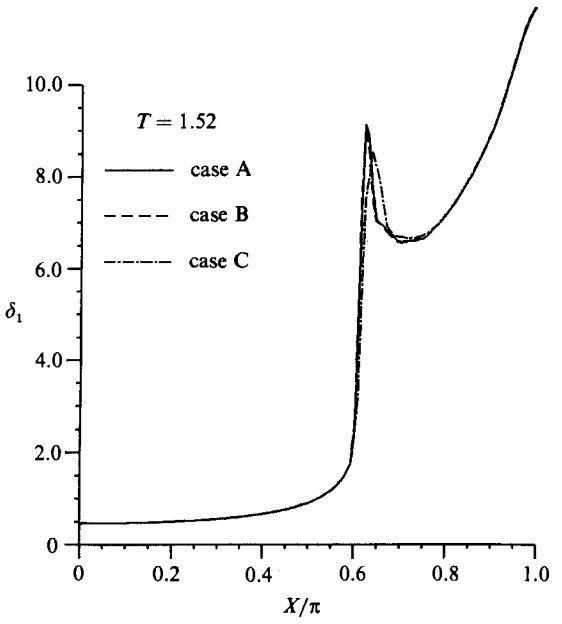

FIGURE 17. Comparison of the profiles of displacement thickness for different grid spacings shown in table 2.

	ΔX	Δt
A	$\frac{1}{128}\pi$	0.004
B	$\frac{1}{128}\pi$	0.002
C	$\frac{1}{64}\pi$	0.008

TABLE 2. Grid spacings used in the examination of their effects

profiles of displacement thickness with exact numerical solutions by Cebeci (1979) for $t = 0.1, 0.3, 0.5, 0.7$ and 1.0 and by van Dommelen & Shen (1980) for $t = 0.7$, 1.0, 1.25 and 1.4. The present result agrees quite well with others, especially for $t < 1.0$, and Cebeci's results are invisible because of overlapping. Figure 16 shows the distribution of skin-friction coefficient at various instants with the results of Cebeci for $t = 0.1, 0.2, 0.5, 1.0$ and 1.25 and those of van Dommelen & Shen for $t = 0.2$, 0.4, 0.6 and 1.0. In figure 17 the effects of grid spacing on the profiles of displacement thickness are examined for three cases shown in table 2. The results for cases A and B coincide in graphical accuracy, and that for case C gives a slightly smaller hump near the singularity because of larger numerical dissipation proportional to Δx. The present method allows integration past the time $t = 1.5$ corresponding to singularity according to van Dommelen & Shen. This means that for $t > 1.5$ the discontinuous profiles, which are weak solutions of the hyperbolic system, are captured numerically by the dissipative finite-difference scheme without blow-up apart from the physical relevance. Using Keller's box method modified by the zigzag differencing scheme when there were reversed-flow regions, Cebeci obtained a solution without singularity for $t < 1.4$. van Dommelen & Shen treated the boundary-layer equations in Lagrangian coordinate using a Crank–Nicolson scheme. The present method, being an efficient

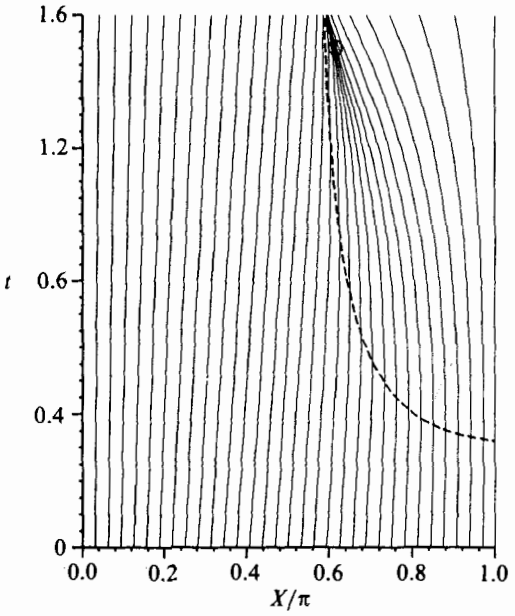

FIGURE 18. Plot of the C_1 characteristics for a circular cylinder impulsively set in motion.

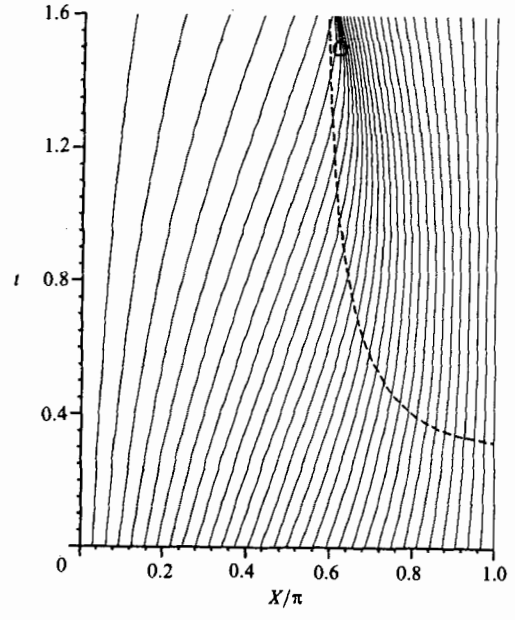

FIGURE 19. Plot of the C_2 characteristics for the circular cylinder.

approximate method, gives excellent results by no means inferior to the exact methods.

In figures 18, 19 and 20 the C_1, C_2, C_3 characteristics are shown by solid lines and the trajectory of the point of vanishing wall shear stress is shown by dashed lines. The open circles in the figures are the stationary points of the Lagrangian dependent variable x found by van Dommelen & Shen and identified with the formation of

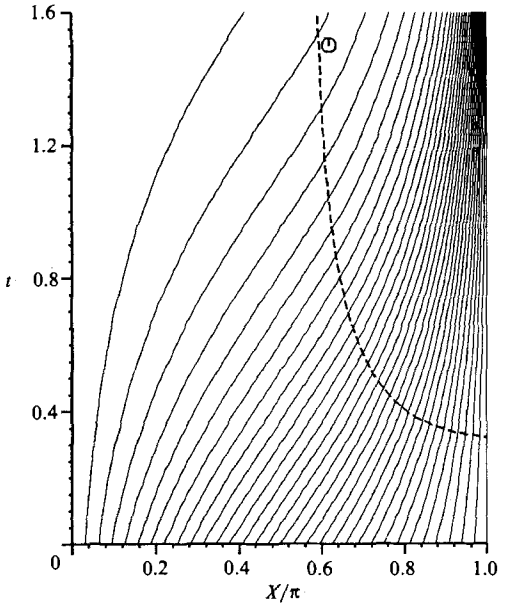

FIGURE 20. Plot of the C_3 characteristics for the circular cylinder.

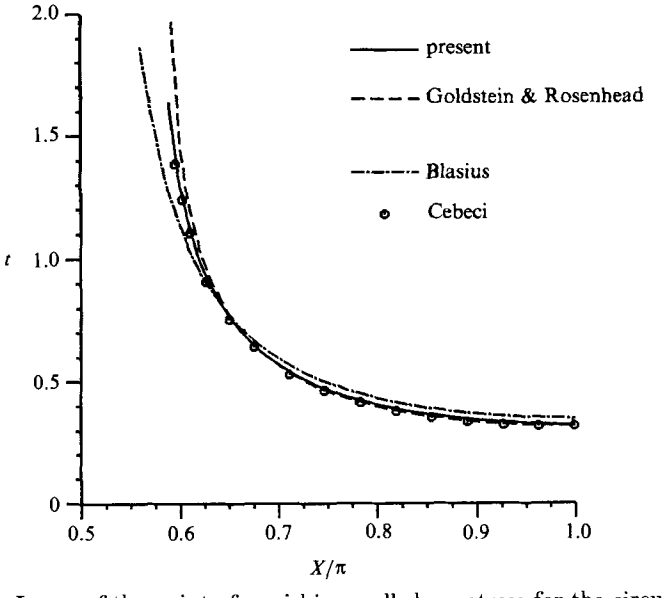

FIGURE 21. Locus of the point of vanishing wall shear stress for the circular cylinder.

separation singularity in unsteady flow. The characteristics C_i are drawn by numerically integrating the equation $\mathrm{d}x/\mathrm{d}t = \lambda_i$ $(i = 1, 2, 3)$, where the values of λ_i are interpolated based on the data on the grid points previously calculated by the finite-difference method. In the attached-flow region, namely the lower or left side of the dashed line, all the characteristics have positive values. Figure 18 shows that λ_1 has negative values in the reversed-flow region, and the locus of $\lambda_1 = 0$ is identified

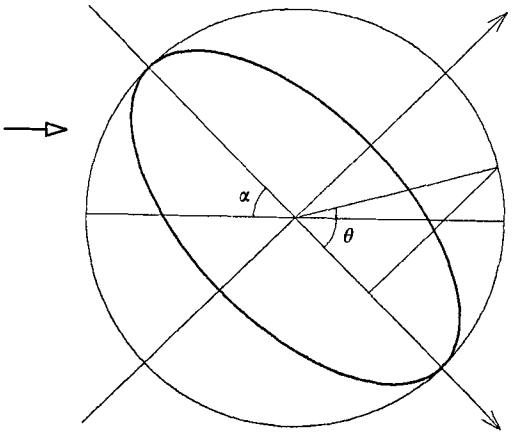

FIGURE 22. Schema of an elliptic cylinder.

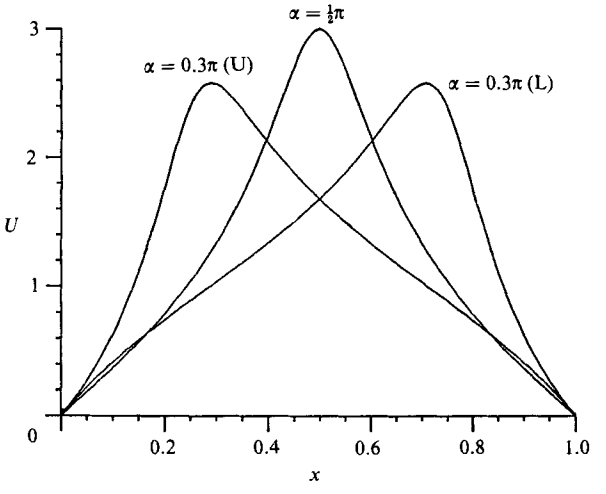

FIGURE 23. Potential-flow velocity distribution on the elliptic cylinder.

with that of vanishing wall shear. Further, the C_1 characteristics family form an envelope very near $x = 0.618\pi$, $t = 1.5$ of van Dommelen & Shen's singular point. In figure 19 C_2 similarly form an envelope, but the locus of $\lambda_2 = 0$ has no definite physical meaning, unlike C_1. In figure 20 C_3 always have positive directions and form no envelope. In figure 21 the locus of the point of vanishing wall shear stress of the present result is compared with those of Cebeci and first-order (Blasius 1908) and second-order (Goldstein & Rosenhead 1936) series solutions. The present result agrees quite well with those of Cebeci and Goldstein & Rosenhead.

5.2. *Elliptic cylinder*

The starting flow of an elliptic cylinder is also investigated by the present integral method. In this problem, like the flows around practical airfoils, leading-edge separation and stall will occur at somewhat larger incidence angle. The contour of an elliptic cylinder of thickness ratio 0.5 is depicted in figure 22. When the incidence

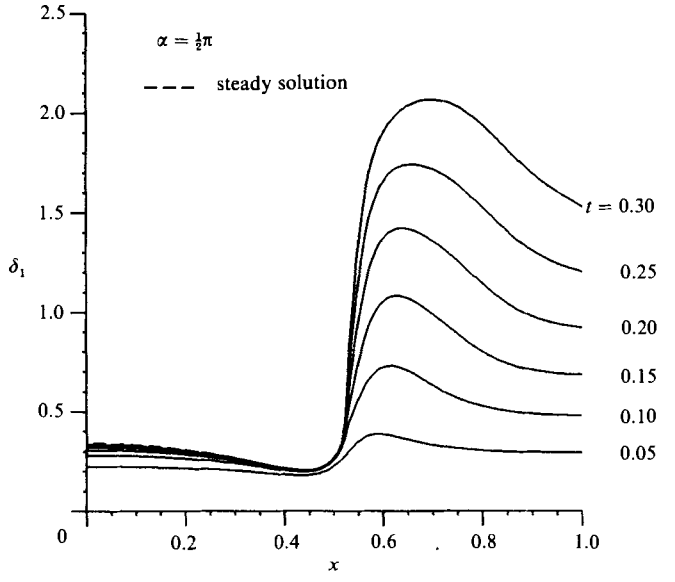

FIGURE 24. Computed results of displacement thickness for the elliptic cylinder impulsively set in motion at the incidence angle $\alpha = \frac{1}{2}\pi$.

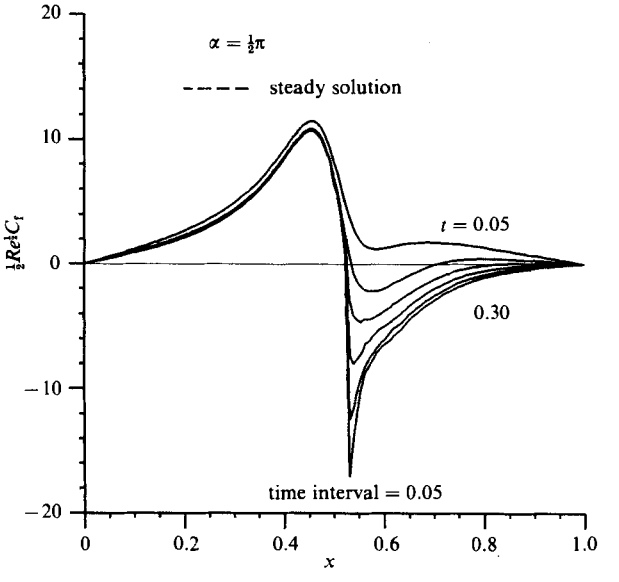

FIGURE 25. Computed results of skin-friction coefficient for an elliptic cylinder at the incidence angle $\alpha = \frac{1}{2}\pi$.

angle is α, the free-stream velocity distribution around the cylinder is given by the potential-flow theory as

$$U = \frac{|3\sin(\theta-\alpha)|}{(4\sin^2\theta+\cos^2\theta)^{\frac{1}{2}}}. \tag{28}$$

The streamwise coordinate x along the body surface is given by

$$x = \left| \int_{\alpha+\pi}^{\theta} [\tfrac{4}{3}(4\sin^2\theta+\cos^2\theta)]^{\frac{1}{2}}\,\mathrm{d}\theta/L \right|, \tag{29}$$

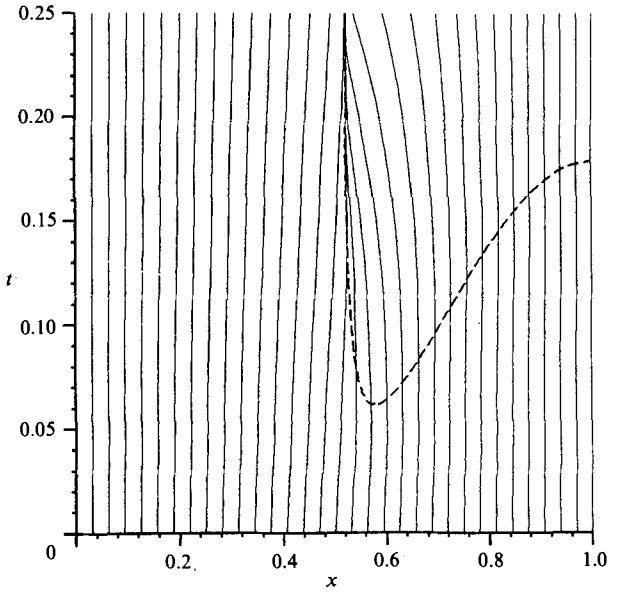

FIGURE 26. Plot of C_1 characteristics (solid lines) and the locus of the point of vanishing wall shear stress (dashed line) for the elliptic cylinder at the incidence angle $\alpha = \frac{1}{2}\pi$.

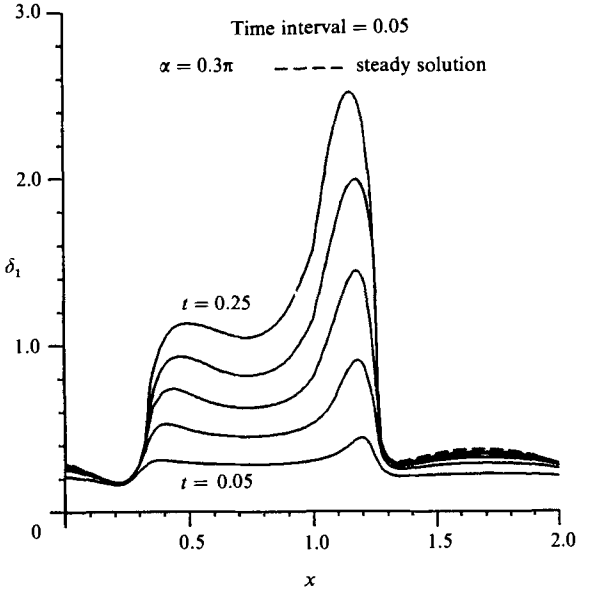

FIGURE 27. Computed results of displacement thickness for the elliptic cylinder at the incidence angle $\alpha = 0.3\pi$.

where the origin of this coordinate is the forward stagnation point $\theta = \alpha + \pi$ and L is a half-circuit length of the cylinder. The free-stream velocity distributions for the incidence angles $\frac{1}{2}\pi$ and 0.3π (upper and lower surface) are shown in figure 23. The initial and boundary condition are the same as in the case of the circular cylinder.

Figures 24–26 show the results when the incidence angle $\alpha = \pi/2$. The time-varying profiles of displacement thickness (figure 24) and skin-friction coefficient (figure 25)

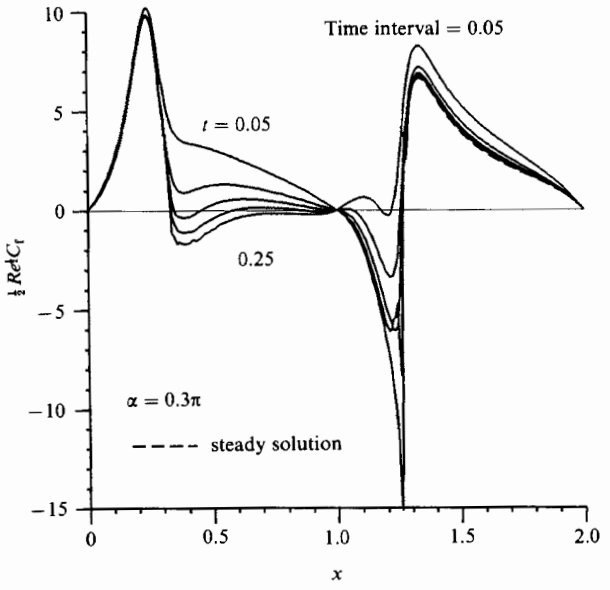

FIGURE 28. Computed results of skin-friction coefficient for the elliptic cylinder at the incidence angle $\alpha = 0.3\pi$.

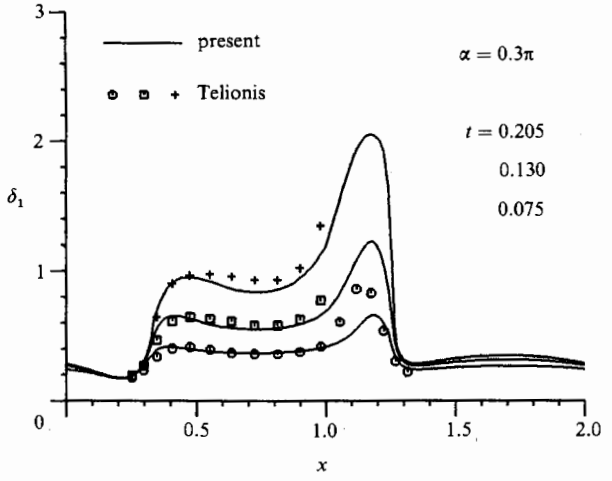

FIGURE 29. Comparison of the displacement thickness with the results of Telionis & Tsahalis (1974) for the elliptic cylinder at the incidence angle $\alpha = 0.3\pi$.

show that in the attached region the boundary layer rapidly converges to the steady solution denoted by dashed lines (hard to see because of overlapping), whereas it continues to develop in the separated region. In figure 26 C_1 characteristics and the locus of the point of vanishing wall shear are shown by solid and dashed lines respectively. A separation bubble appears at $t = 0.06$, then grows larger and finally coalesces with the other symmetric one at $t = 0.19$. The envelope of the characteristics is formed at the forward zero-wall-shear point prior to the coalescence of the bubbles. Figures 27–32 show the results when the incidence angle $\alpha = 0.3\pi$. Since the flow field becomes asymmetric, the calculations on the upper surface ($0 < x < 1$) and the lower

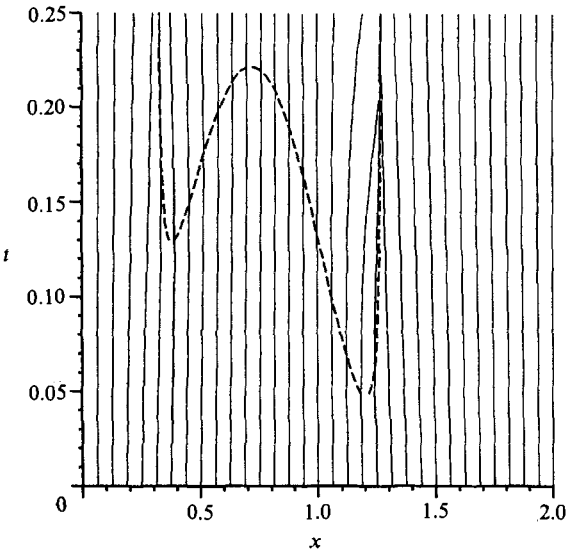

FIGURE 30. Plot of C_1 characteristics (solid lines) and the locus of the point of vanishing wall shear stress (dashed line) for the elliptic cylinder at the incidence angle $\alpha = 0.3\pi$.

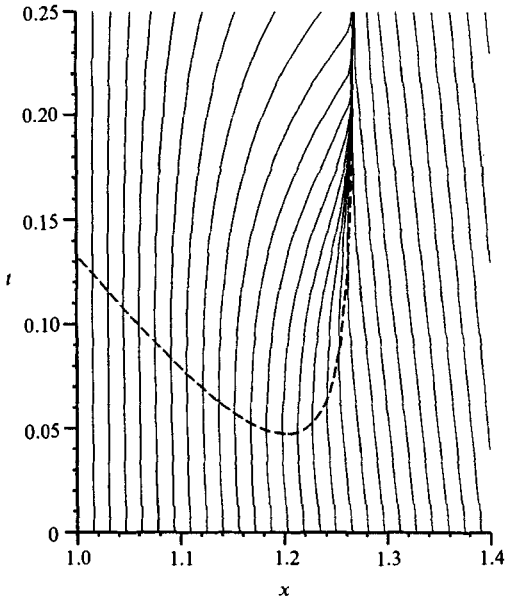

FIGURE 31. The detailed C_1 characteristics in the neighbourhood of focusing on the lower surface of the elliptic cylinder at the incidence angle $\alpha = 0.3\pi$.

surface ($1 < x < 2$) were performed separately and the results were plotted successively. All of them match perfectly at the rear stagnation point $x = 1, \theta = 0.3\pi$. Figures 27 and 28 show the time-varying profiles of displacement thickness and skin-friction coefficient plotted at regular time intervals. Figure 29 compares the present results with those of Telionis & Tsahalis (1974). In figure 30 the locus of the point of vanishing wall shear shows that a separation bubble firstly appears on the

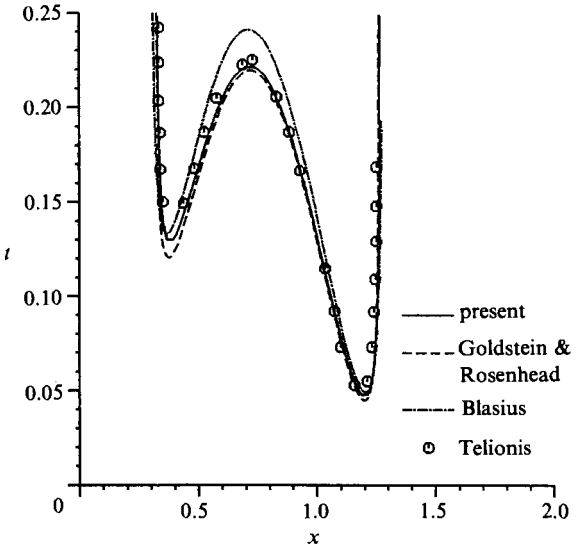

FIGURE 32. Locus of the point of vanishing wall shear stress for the elliptic cylinder at the incidence angle $\alpha = 0.3\pi$.

lower surface at $t = 0.045$, subsequently on the upper surface at $t = 0.13$, and finally they coalesce at $t = 0.22$. Figure 31 show the detailed C_1 characteristics in the neighbourhood of focusing on the lower surface. Figure 32 compares the locus of the point of vanishing wall shear stress. The present result agrees well with that of Telionis and Goldstein & Rosenhead.

6. Conclusions

A two-parameter integral method has been presented which is applicable even to separated boundary layers. The governing equation system, which consists of three moment equations of the boundary-layer equation, was confirmed to be classified as a quasi-linear hyperbolic system under the assumed velocity-profile families. It was numerically solved by a dissipative finite-difference scheme in order to capture a discontinuous solution associated with the singularity of unsteady separation. The generation of the singularity was ascertained as formation of the envelope of the characteristics which were drawn based on the calculated results of the shape parameters. The starting flows of a circular and an elliptic cylinder were considered as definite examples. The present method was proved to give excellent results, in comparison with the exact methods, not only for practically important boundary-layer quantities, such as displacement thickness or skin-friction coefficient, but also for generation of separation singularity.

Professor I. Tani is thanked for his helpful comments on the work.

REFERENCES

BLASIUS, H. 1908 *Z. Math. Phys.* **56**, 1.

CEBECI, T. 1979 *J. Comp. Phys.* **31**, 153.

CEBECI, T. 1982 In *Numerical and Physical Aspects of Aerodynamic Flows* (ed. T. Cebeci), chap. 15. Springer.

CEBECI, T. & WILSON, W. B. 1972 *Trans. ASME* D: *J. Basic Engng* **94**, 697.

COUSTEIX, J. & HOUDEVILLE, R. 1981 *AIAA J.* **19**, 976.

COWLEY, S. J. 1983 *J. Fluid Mech.* **135**, 389.

GOLDSTEIN, S. 1948 *Q. J. Mech. Appl. Maths* **1**, 43.

GOLDSTEIN, S. & ROSENHEAD, L. N. 1936 *Proc. Camb. Phil. Soc.* **32**, 392.

HOWARTH, L. 1938 *Proc. R. Soc. Lond.* A **164**, 547.

LEES, L. & REEVES, B. L. 1964 *AIAA J.* **2**, 1907.

LUGT, H. J. & HAUSSLING, H. J. 1974 *J. Fluid Mech.* **65**, 711.

MATSUSHITA, M. & AKAMATSU, T. 1983 *Bull. JSME* **26**, 1502.

MATSUSHITA, M. & AKAMATSU, T. 1984 *Bull. JSME* (to appear).

MOSES, H. L., JONES, R. R. & O'BRIEN, W. F. 1978 *AIAA J.* **16**, 61.

NAGATA, H., MINAMI, K. & MURATA, Y. 1979 *Bull. JSME* **22**, 512.

POHLHAUSEN, K. 1921 *Z. angew. Math. Mech.* **1**, 252.

PROUDMAN, I. & JOHNSON, K. 1962 *J. Fluid Mech.* **12**, 161.

SATOFUKA, N. & MORINISHI, K. 1982 *NASA TM* 81339.

SCHUH, H. 1953 *Z. Flugwiss.* **1**, 122.

SEARS, W. R. & TELIONIS, D. P. 1975 *SIAM J. Appl. Maths* **28**, 215.

SHEN, S. F. 1978 *Adv. Appl. Mech.* **18**, 177.

TANI, I. 1954 *J. Aero. Sci.* **21**, 487.

TANI, I. & YU, N. J. 1971 In *Recent Research on Unsteady Boundary Layers* (ed. E. A. Eichelbrenner), p. 886.

TA PHUOC LOC 1980 *J. Fluid Mech.* **100**, 111.

TELIONIS, D. P. 1981 *Unsteady Viscous Flows.* Springer.

TELIONIS, D. P. & TSAHALIS, D. T. 1974 *Acta Astronautica* **1**, 1487.

TERRIL, R. M. 1960 *Phil. Trans. R. Soc. Lond.* A **253**, 55.

VAN DOMMELEN, L. L. & SHEN, S. F. 1980 *J. Comp. Phys.* **38**, 125.

VAN DOMMELEN, L. L. & SHEN, S. F. 1982 In *Numerical and Physical Aspects of Aerodynamic Flows* (ed. T. Cebeci), chap. 17. Springer.

WANG, K. C. 1982 In *Numerical and Physical Aspects of Aerodynamic Flows* (ed. T. Cebeci), chap. 16. Springer.

WILLIAMS, J. C. 1977 *Ann. Rev. Fluid Mech.* **9**, 113.

WILLIAMS, J. C. 1982 *J. Fluid Mech.* **115**, 27.